RSC Advances

ROYAL SOCIETY OF CHEMISTRY

www.rsc.org/advances

Table of Contents

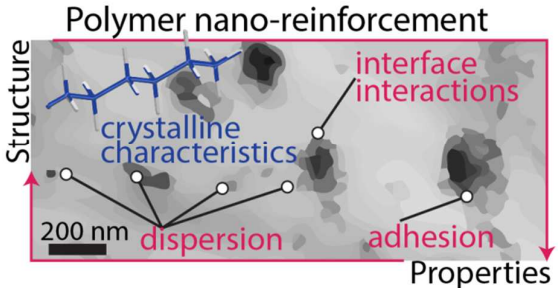

A systematic evaluation of the factors governing the measured thermal and mechanical properties reinforcement in crosslinked polyethylene nanocomposites is presented.

Journal Name

RSCPublishing

ARTICLE

Understanding the mechanical and thermal properties reinforcement of crosslinked polyethylene by nanodiamonds and carbon nanotubes

Cite this: DOI: 10.1039/x0xx00000x

Received 00th January 2012,
Accepted 00th January 2012

DOI: 10.1039/x0xx00000x

www.rsc.org/

E. Roumeli [a], A. Avgeropoulos [b], E. Pavlidou [a], G. Vourlias [a], Th. Kyratsi [c], D. Bikiaris [d] and K. Chrissafis [a]

A comprehensive investigation of the mechanical and thermal properties reinforcement of silane-crosslinked polyethylene nanocomposites, containing small amounts of multi-walled carbon nanotubes (MWCNTs) and nanodiamonds (NDs), is presented in this work. Lower filler concentrations allowed a satisfactory dispersion, enabling the successful reinforcement of the matrix in every aspect. As the nanofiller content increased, the formed aggregates enlarged and the performance of the composites became more brittle. The measured stiffness enhancement of all the composites was found to be mainly influenced by the crystalline characteristics of the matrix and filler-matrix adhesion. Moreover, it was concluded that filler dispersion and filler-matrix interactions govern the ultimate strength and toughness behavior of these composites, which were found to slightly increase in minimum filler concentrations. Fractography was employed to study the embrittleness of the composites with higher filler loadings, and the observations revealed that a ductile to brittle transition is caused by a micro-deformation mechanism change in these composites. Furthermore, the prepared composites had a significantly improved thermal conductivity, which was mainly related to their superior specific heat capacity, while a great thermal stability enhancement was also revealed.

Introduction

Polymer materials reinforcement using nanofillers has been a topic of intense research and much deliberation in the past decade [1-7]. The incorporation of small amounts of nanoparticles, nanotubes, nano-platelets or other nano-sized materials in polymers, has opened an exciting new field for both academic and industrial research. Since the first reports of significant mechanical and thermal properties reinforcement of polymers due to the incorporation of nanoparticles [8] a global quest for methods that could enable a successful transfer of the outstanding properties nanofillers to polymer matrices began. In this context, carbon nanomaterials like multi-walled carbon nanotubes (MWCNTs) have been extensively examined as reinforcing fillers due to their outstanding mechanical performance, thermal and electrical conductivity [9-12].

The cornerstone of all these efforts is the thorough and systematic investigation of micro-structure property relationships in the produced nanocomposites [5, 13-19]. After such a study has been performed, the corresponding hybrids or composites could be re-designed in order to yield materials of preferred performance. Nevertheless, fundamental reports on factors influencing nanocomposites' reinforcement are rather rare and even more so, in polymer nanocomposites.

It has been established that the polymer's crystal structure, molecular weight distribution and macromolecular chain conformation among others, can greatly influence its mechanical properties [20-23], while filler dispersion, purity and adhesion can govern its reinforcement [24-27]. Noteworthy progress has also been made in the area of configuring the macromolecular conformation around the nanofiller-rich regions within the matrix, in which different chain dynamics have been reported and therefore, can be crucial to the final reinforcement of the composite [28-32].

In the present work, we prepared a series of silane-crosslinked high density polyethylene (PEX) nanocomposites containing small amounts of MWCNTs and nanodiamonds (NDs) using melt-mixing. The mechanical performance and thermal properties of the prepared composites were thoroughly investigated in order to determine the factors governing their final performance. The measured significant stiffness improvement was related to the presence of the filler as well as polymer's microstructural characteristics and filler dispersion and adhesion, while the outstanding thermal conductivity and thermal stability enhancements were related to the presence of the fillers, their geometry, dispersion and interactions with the matrix.

Experimental

Materials and methods

Materials. Purified multi-walled carbon nanotubes (MWCNTs) were purchased from Chengdu Organic Chemicals Co. Ltd. The inner and outer diameters of MWCNTs were less than 8 nm and 2-5 nm respectively and they have 2.1 g/cm^3 density. NDs were purchased from the International Technology Center (North Carolina, USA) and have an average primary particle size of 4 nm.
Polyethylene's crosslinking was performed following the two-step silane grafting and water curing process [33]. High density polyethylene (HDPE) grafted with vinyl trimethoxysilane (VTMS) (HDPE-g-VTMS) was kindly supplied by Sioplas S.A. Sioplas S.A. and exhibited the following characteristics: average molecular weight per number, $\bar{M}_n$=28000 g/mol; average molecular weight per weight, $\bar{M}_w$=120200 g/mol and intrinsic viscocity, [η]=1.54 dl/g. A catalyst masterbatch containing the same HDPE along with dibutyltin dilaurate (DBTDL), internal lubricants, stabilizers and various antioxidants was also supplied by Sioplas S.A. The catalyst, in the step of curing in water at 90^{o}C for 24 h, accelerates the hydrolysis reaction of the grafted silyl groups and the subsequent condensation of silanols to form siloxane bonds.

Nanocomposites preparation. Prior to melt mixing, solid state ball milling was employed in order to achieve a fine dispersion of the nanofillers in the polymer matrix. Mixtures of 95 parts of HDPE-g-VTMS, 5 parts of catalyst masterbatch and 1, 2, 3 and 5 wt% MWCNTs with 1,3 and 5 wt% NDs and were solid-state mixed in a Retsch centrifugal ball mill (model S 100) for 6 hours in a rotation speed of 500 rpm. Each mixture was afterwards melt-mixed in a Haake-Buchler Rheomixer (model 600) with roller blades and a mixing head with a volumetric capacity of 69 cm^3. For this case, 10 minute mixing at 200^{o}C with a torque speed of 60 rpm was used. The prepared samples were immediately hot pressed using an Otto Weber, Type PW 30 hydraulic press connected with an Omron E5AX Temperature Controller, at a temperature of 180±5^{o}C under 50-100 kN, in order to prepare films of 10-30 μm and 350-450 μm thickness appropriate for each type of measurement. The films were rapidly cooled by immersion in water at 25^{o}C. Finally, all prepared films were exposed to a hot bath (90^{o}C water for 24 hours) to complete the crosslinking process in the bulk of the polymer as previously reported [33].

Mechanical properties. Mechanical properties testings were performed on an Instron 3344 dynamometer, in accordance with ASTM D638 using a cross-head speed of 50 mm/min. Sheets of about 350-450 μm thickness were used, prepared as described previously. In order to measure the mechanical properties from these sheets, dumb-bell-shaped tensile test specimens (central portions 5 × 0.5 mm thick, 22 mm gauge length) were cut in a Wallace cutting press. At least five measurements were conducted for each sample, and the results were averaged to obtain a mean value. The values of elastic modulus, tensile strength at yield and at break point and elongation at break were experimentally determined. The toughness was calculated from the area under the obtained stress-strain curves as described elsewhere [34].

Scanning electron microscopy (SEM). The morphology of the failure surfaces of all nanocomposites after tensile testing were examined in a SEM system (JEOL JSM 840A-Oxford ISIS 300 microscope). The specimens were carbon coated in order to provide good conductivity of the electron beam. Operating conditions were: accelerating voltage 20 kV, probe current 45 nA, and counting time 60 s.

X-ray diffraction (XRD). The XRD patterns of the prepared materials (10-30 μm thick) were recorded by a water-cooled Rigaku Ultima$^+$ diffractometer using CuKa radiation, a step size of 0.02^o and a step time of 3 s, operating at 40 kV and 30 mA.

Crystallinity calculations of the studied materials were performed by fitting the XRD profiles at the area of 10^o<2θ<40^o with Gaussian-Lorentzian Cross Product curves and incorporating the fitting parameters in the following expression [35]:

$$\omega_c\% = \frac{A_{cr}}{A_{cr} + A_{am}} \times 100\% \quad (1)$$

where the crystalline and amorphous peak areas are noted as A_{cr} and A_{am} respectively.

Transmission electron microscopy (TEM). Ultra-thin film samples of the nanocomposites were prepared through cryo-microtoming at -90oC with a DIATOME cryo-45^o diamond knife by the ultra-microtome Leica EM FC7. TEM images of the thin sections were placed on copper grids and studied using a JEOL 120 CX microscope operating at 120 kV.

Differential Scanning Calorimetry (DSC). DSC measurements have been performed in a DSC141 (Setaram). The instrument was temperature and energy calibrated using high-purity Zinc, Tin and Indium. Samples of 6 mg were placed in aluminium sealed crucibles, while an identical empty crucible was used as reference in each measurement. The samples were heated from ambient temperature (25oC) to 220^{o}C at 5^{o}C/min in a 50 ml/min flow of N_2, then held at 200^{o}C for 5 min, cooled to 60^{o}C with a cooling rate of 5^{o}C/min and then heated again with the same heating rate. The second heating data were used for evaluation.
An estimation of crystal size (l_c) was obtained from the DSC data using the Thomson-Gibbs equation [36]:

$$T_m = T_m^0\left(1 - \frac{2\sigma_e}{l_c \rho_c \Delta H_m^0}\right) \quad (2)$$

Where T_m and T_m^0 are the experimental and equilibrium melting peak temperatures respectively (T_m^0 taken 145.7^{o}C [37]), σ_e is the fold surface free energy (9.3·10^6 J/cm^2 for polyethylene [38]), ΔH_m^0 is the theoretical melting enthalpy per unit volume for totally crystalline polyethylene (taken 293 J/cm^3 [37]) and ρ_c is the totally crystalline polyethylene density (taken 1000 kg/m^3 [36]).

Thermal conductivity measurements using laser flash analysis (LFA) and temperature modulated differential scanning calorimetry (TMSDC). Thermal conductivity measurements were performed using a Laser Flash Analysis instrument (LFA 457, Netzsch). Samples were cut into (10 × 10) mm squares with 0.4 mm thickness and were coated with 5 μm of graphite. All measurements were taken at 50^{o}C with a laser voltage power of 2786 V and a laser transmission filter of 100%. A total of 10 shots per sample set were taken. All curves were fitted using a variety of models in order to determine the most suitable for each material.
In addition, the heat capacity of each sample was determined by temperature modulated differential scanning calorimetry (DSC

Q 200, TA Instruments). The samples were heated from 25 °C to 95 °C with an underlying heating rate of 2.5°C/min, modulation amplitude of 0.53 oC and a period of 80 s. The value of specific heat capacity at 50°C was obtained for all the studied materials and used for the determination of thermal conductivity. The thermal conductivity specifically at 50°C was selected as an intermediate operating temperature in a geothermal piping system.

Thermogravimetry (TG). Thermogravimetric (TG) analysis was carried out with a Setsys 16/18 TG-DTA (Setaram). Samples (4±0.2 mg) were placed in alumina crucibles. An empty alumina crucible was used as reference. Samples were heated from ambient temperature to 600°C at 20°C/min in a 50 ml/min flow of N_2.

Contact angle and surface analysis. Thermogravimetric Water and diiodomethane (CH_2I_2) contact angle measurements of the prepared materials were measured at room temperature by the sessile drop method using a Data Physics OCA 30 device. The measured contact angle values presented in this work are the arithmetic mean of six-twelve measurements. The subsequent specific free energy analyses were performed using the methods proposed by Fowkes and Wu [25, 39].

Fowkes' theory [25] is based on two fundamental assumptions: that surface forces and energies are additive and that a geometric mean can be used for the work of adhesion for each type of force/energy. According to that method, the surface free energy (γ) of the solid (subscript, *s*), liquid (subscript, *l*) and their corresponding polar and dispersive contributions (superscripts *p* and *d* respectively) are related with the measured contact angle (θ) by the following expression:

$$\gamma_L\left(1+\cos\theta\right)=2\left[\left(\gamma_L^p\gamma_s^p\right)^{1/2}+\left(\gamma_L^d\gamma_s^d\right)^{1/2}\right] \quad (3)$$

Other theories have also been proposed falling under the same concept but approaching the problem with alternative mathematical principles. One of the most widely accepted methods for polymer interfacial energy calculations, proposed by Wu [39], combines by a harmonic mean equation the polar and dispersive forces found in polymer matrices. It is based on the following equation applied for 2 liquids of different polarity:

$$\left(1+\cos\theta\right)\gamma_L=4\left[\frac{\gamma_L^d\gamma_s^d}{\gamma_L^d+\gamma_s^d}+\frac{\gamma_L^p\gamma_s^p}{\gamma_L^p+\gamma_s^p}\right] \quad (4)$$

Using both these methods, the specific free energy and its contributions from polar and dispersive forces respectively were evaluated for all the nanocomposites. Moreover, using Girifalco-Good's formula, the interaction parameter (φ) was determined from the following equation [40].

$$\varphi=\frac{\gamma_L\left(1-\cos\theta\right)}{2\sqrt{\gamma_S\gamma_L}} \quad (5)$$

Results and discussion

Morphology and dispersion

TEM images of the prepared nanocomposites are presented in Fig. 1. Views of the 1 wt% MWCNTs/5 wt% NDs composite are presented in Fig. 1a-b, revealing an overall fine dispersion of the particles in the matrix. From these images it can also be seen that NDs aggregations were sized between 30-300 nm and nanotubes were either embedded in those aggregates or interconnecting them (as indicated by black and red arrows respectively in Fig.1). Also some nanotubes were found to be standing alone, apart from the filler aggregates (marked with white arrows in Fig.1a-b). In Fig. 1c a view from the 2 wt% MWCNTs/1 wt% NDs composite is presented, revealing a variety of differently sized nanofillers aggregations. Small NDs aggregates from 15-45 nm were found along with rather large NDs/MWCNTs aggregates sized from a few hundred nanometers to almost 1 μm. Even so, the dispersion of the formed aggregates is considered rather satisfying.

In Fig. 1d-f images of the PEX/3 wt% MWCNTs/5 wt% NDs composites are presented. Large NDs/MWCNTs arrays from 200 to 600 nm could be distinguished throughout the whole section. In Fig. 1e-f particularly, some really small NDs aggregations (10-25 nm) were revealed, while most of the NDs present in the section were accumulated in large aligned arrays of 100 nm - 1 μm. A closer observation of the arrayed nanofillers reveals that some MWCNTs are embedded in NDs aggregates (indicated by black arrows) while most of them are arrayed separately in the space between NDs aggregations (indicated by white arrows).

In Fig. 1g-h images of the PEX/5 wt% MWCNTs/3 wt% NDs and PEX/5 wt% MWCNTs/5 wt% NDs composites are presented respectively. The large filler aggregates formation seems inevitable through these images. Both small and rather large filler aggregations can be distinguished. Some single MWCNTs are found to be lying in the matrix (indicated by white arrows), while most of them were again found to be embedded within the large NDs aggregations (indicated by black arrows).

Thus, from the microscopy observations, it was found that while low filler concentrations allow a satisfying dispersion, when their concentration increases, the composites are dominated by large filler aggregations. Therefore, as filler dispersion is a crucial factor which quite often determines the matrix reinforcement, an overall more significant improvement is expected in the lower filler concentrations.

Mechanical properties

In Table 1 the mechanical properties of all the prepared composites are presented. Generally, in all the studied properties, a decreasing trend with increasing NDs content can be observed. Selected stress-strain curves of all the mixed nanocomposites are presented in Fig. 2. The incorporation of both types of nanofillers was expected to improve the elastic modulus and the yield strength of the matrix as a direct result of their superior stiffness. A stiffness reinforcement is indeed observed in all the prepared nanocomposites. In details, the elastic modulus of the mixed nanocomposites with the lowest amount of NDs (1-5 wt% MWCNTs/1 wt% NDs) is enhanced with increasing MWCNTs loading. In order to estimate the effect of the participation of both types of fillers into PEX versus the effects of each type of filler separately, we need to take into account that when only MWCNTs were incorporated into PEX [41], a great stiffness enhancement was found for the 0.5 wt% composite which was retained at the 1-3 wt% composites. This enhancement was even greater in the 5 wt% composite. When only NDs were incorporated into PEX [42], an initial great stiffness enhancement was obtained for low NDs content, which was found to be decreasing with increasing filler content. In the mixed nanocomposites, as NDs content increases, the elastic modulus of the composites monotonously decreases. On the contrary, increasing MWCNTs concentration leads

to enhanced elastic modulus values of the corresponding mixed composites. Therefore, it seems that the separate effects found on one-filler-type-composites, were transferred to the mixed composites. The mixed composites with 5 wt% MWCNTs/1 wt% NDs, 3 wt% MWCNTs/1 wt% NDs and 5 wt% MWCNTs/3 wt% NDs had the highest elastic modulus of the mixed composites.

In the composites with only NDs, a monotonously decreasing trend for the yield stress was found with increasing NDs concentration. This behavior is also found in every set of mixed composites. The composite with 2 wt% MWCNTs/1 wt% NDs had the highest yield strength compared to all the mixed composites, which is 12.7 MPa higher than the neat polymer's. The observed total stiffness reinforcement (factoring in both the elastic modulus and the yield strength) was found to be more significant in the 2 wt% MWCNTs/1 wt% NDs, 5 wt% MWCNTs/1 wt% NDs and 3 wt% MWCNTs/1 wt% NDs.

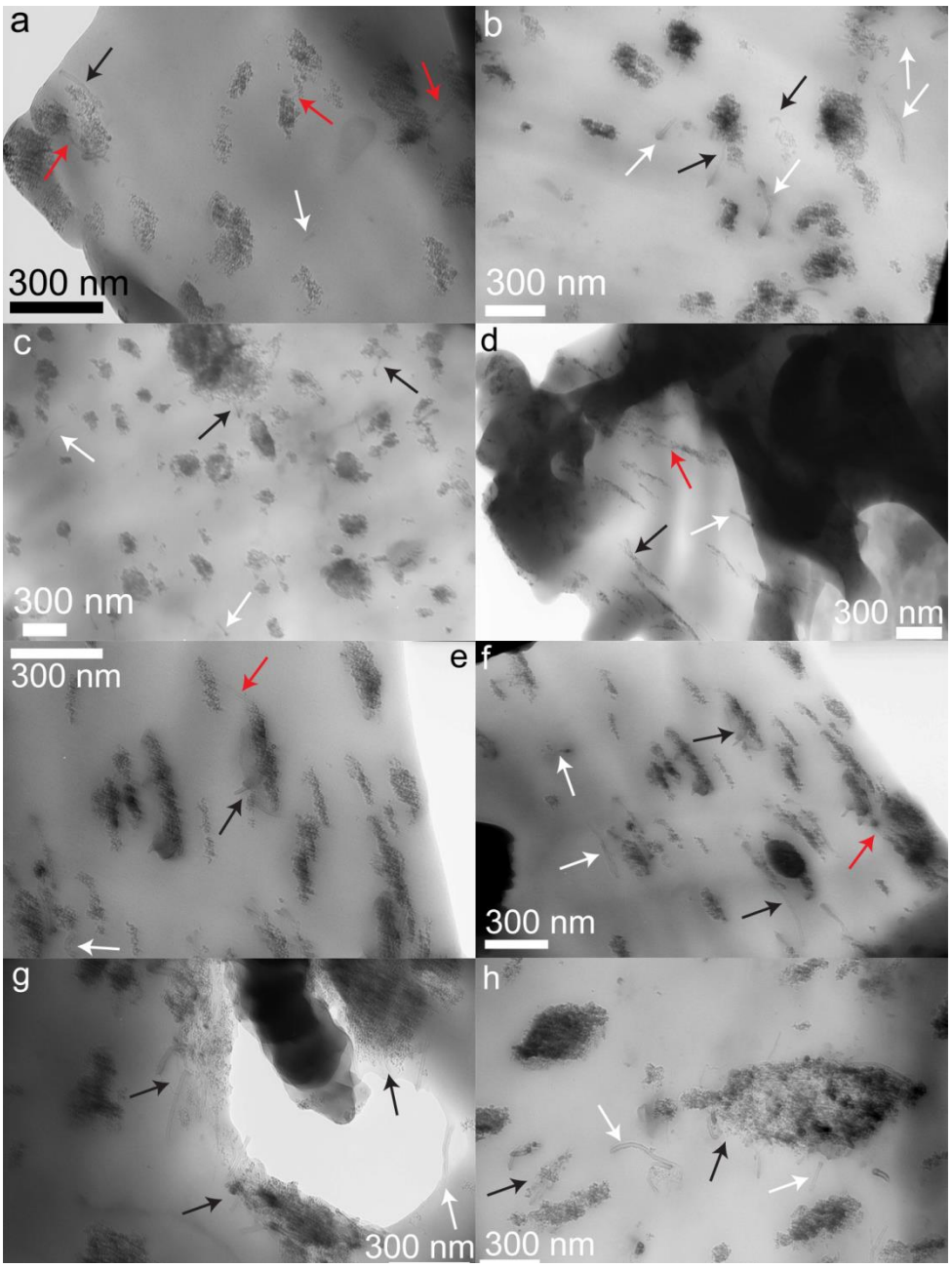

Fig.1. TEM micrographs of PEX nanocomposite containing (a-b) 1 wt% MWCNTs/5 wt% NDs, (c) 2 wt% MWCNTs/1 wt% NDs, (d-f) 3 wt% MWCNTs/5 wt% NDs, (g) 5 wt% MWCNTs/3 wt% NDs and (h) 5 wt% MWCNTs/5 wt% NDs. Coloured arrows indicate MWCNTs embedded in the nanofiller aggregates (black), interconnecting the aggregated (red) and standing alone in the matrix (white).

Our previous findings regarding the strength at break of PEX nanocomposites indicate that the incorporation of a low amount of MWCNTs in PEX leads to a significant reinforcement, while for higher loadings the strength of the composites is almost the same as neat PEX. Furthermore, the incorporation of NDs leads to an even more significant ultimate strength reinforcement for the lowest concentrations, but as their content increases, the reinforcement monotonously decreases, reaching values notably lower than PEX.

In the mixed composites, increasing NDs content tends to monotonously decrease their ultimate strength, while a similar effect was found with increasing MWCNTs content. Therefore, the composites with the lowest amounts of MWCNTs and NDs have the highest strength at break, which is lower in any case that the corresponding strength of the composites with only one type of filler [41, 42]. Besides that, the strength of all the composites, except the one with 1% MWCNTs -1% NDs, is lower compared to neat PEX.

Table 1. Mechanical properties of all the prepared nanocomposites.

Material	Elastic Modulus (MPa)	Stress at Yield (MPa)	Stress at Break (MPa)	Elongation at Break (%)	Toughness (J/m^3)
Neat PEX	675 ± 35	19.8 ± 0.5	22 ± 2.0	420 ± 21	1893 ± 151
1 wt% MWCNTs – 1 wt% NDs	765.5 ± 9	24.0 ± 0.9	23.0 ± 1.8	460 ± 40	2003 ± 100
1 wt% MWCNTs – 3 wt% NDs	745 ± 17	22.8 ± 0.4	17.9 ±0.9	341 ± 10	1305 ± 20
1 wt% MWCNTs – 5 wt% NDs	736 ± 11	22.5 ± 0.5	17.2 ± 0.8	288 ± 65	1230 ± 20
2 wt% MWCNTs – 1 wt% NDs	785 ± 28	32.5 ± 0.8	20.7 ± 3.1	379 ± 100	1510 ± 50
2 wt% MWCNTs – 3 wt% NDs	770 ± 54	24.4 ± 2.0	17.5 ± 2.3	288 ± 20	1280 ± 55
2 wt% MWCNTs – 5 wt% NDs	730 ± 25	23.7 ± 0.9	16.2 ± 0.8	240 ± 60	1011 ± 100
3 wt% MWCNTs – 1 wt% NDs	795.5 ± 16	24.3 ± 1.4	18.6 ± 1.4	350 ± 20	1398 ± 520
3 wt% MWCNTs – 3 wt% NDs	754.3 ± 30	23.3 ± 0.8	16.4 ± 0.5	246 ± 40	1130 ± 100
3 wt% MWCNTs – 5 wt% NDs	722 ± 17	22.6 ± 0.9	15.4 ± 0.2	195 ± 80	960 ± 100
5 wt% MWCNTs – 1 wt% NDs	808 ± 13	24.6 ± 0.9	18.3 ± 0.9	215 ± 60	910 ± 100
5 wt% MWCNTs – 3 wt% NDs	780 ± 25	23.4 ± 0.1	16.0 ± 1.4	180 ± 5	825 ± 50
5 wt% MWCNTs – 5 wt% NDs	756 ± 6	22.9 ± 0.3	16.2 ± 0.6	165 ± 35	800 ± 50

The elongation at break values clearly decrease with increased MWCNTs and NDs contents. However they are higher compared to the composites with the corresponding amount of MWCNTs [41], but lower than those with the corresponding NDs concentration [42]. This fact highlights that the presence of spherical NDs does help in maintaining a high level of plasticity, but the presence of elongated MWCNTs is bound to interfere with that effect, leading to drastic reductions of the possible elongation prior to failure. This may be due to fact that the shape of MWCNTs and their aggregates is more irregular than that of NDs and penetrates more bulk polymer area, resulting in more nanoconfined regions in which the macromolecular chains have disturbed functionality and dynamics and therefore more of them cannot follow their normal deformation route [30, 43, 44]. The same conclusion can be drawn if the MWCNTs incorporation into PEX is seen through the prism of the far more defects caused in the matrix, as the MWCNTs penetrate more crystallites than NDs.

Considering the observed strength at yield, strength at break and elongation at break behaviors, the toughness behavior can be justified. The nanocomposites with the lowest MWCNTs content (1-2 wt%) and 1 wt% NDs have the highest toughness, which is decreasing with increasing NDs loading. Nonetheless, only the nanocomposite with 1 wt% MWCNTs and 1 wt% NDs has higher toughness than neat PEX. The composites with higher MWCNTs content have much lower toughness which is again decreasing with increasing NDs concentration. The inferior toughness of the composites with increased filler concentrations, which can also be seen through the selected stress-strain curves in Fig. 2, points to a ductile to brittle transition on their fracture behavior. The higher filler content results in a notably more brittle deformation response. Therefore, from the tensile testing results, a possible deformation mechanism change can be proposed as the main reason for the observed ductile to brittle transition of the composites [20, 27, 43, 45, 46]. As a possible deformation mechanism change can be revealed through fractography images, a thorough examination of the composites' fractured surfaces was performed and will be presented in the following section.

The tensile testing findings suggest that when MWCNTs and NDs are incorporated into PEX, the stiffness of the matrix is significantly increased but the ultimate strength and toughness are only slightly increased in the case of the minimum filler concentrations in which filler dispersion was found to be better. As the nanofiller content increases, the fracture performance of the composites becomes more brittle. Even though all the mixed composites had a notably higher stiffness compared to neat PEX, their overall reinforcement was less significant compared to the composites with only one type of filler. The different stiffness and toughness behavior of the nanocomposites suggests that these properties are probably also influenced by different factors besides the presence of the fillers and their dispersion. In the following sections, the matrix crystalline characteristics along with filler dispersion and adhesion effects on the mechanical properties of the mixed nanocomposites will be evaluated and a thorough examination of the fracture behavior of the composites will be presented.

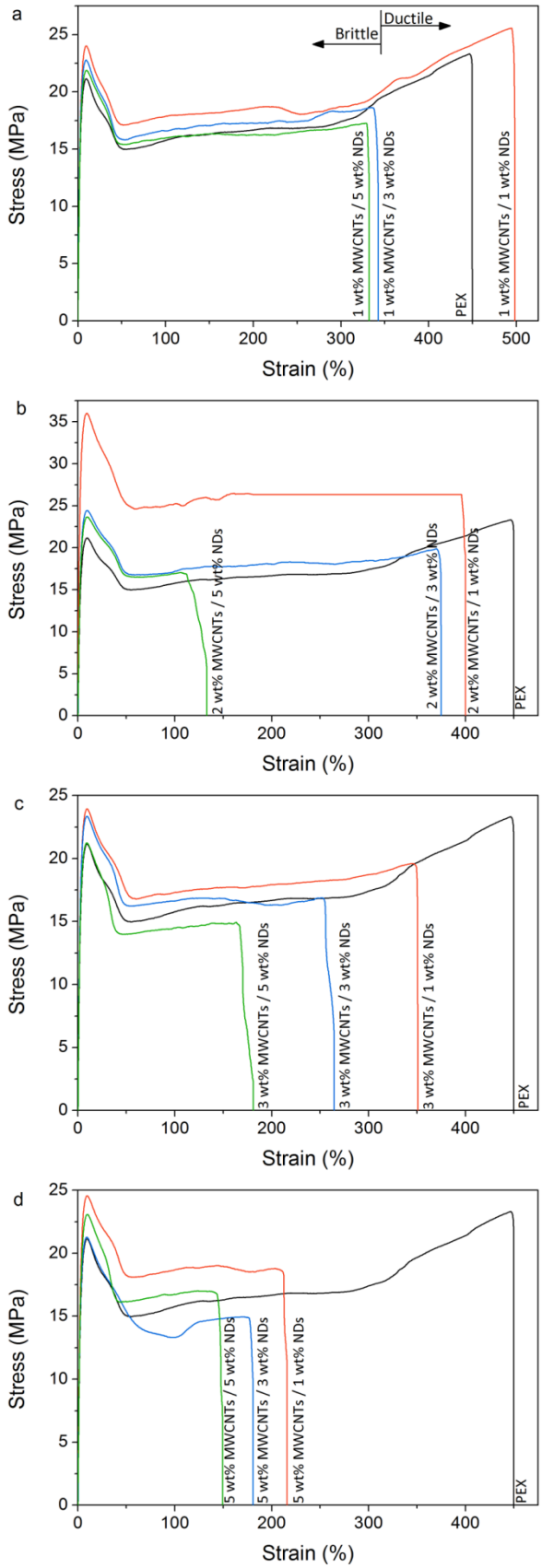

Fig. 2. Characteristic stress-strain curves of PEX and all its prepared composites.

Structural characteristics and molecular conformation effects on the mechanical properties of the composites

As already mentioned, the mechanical properties reinforcement of nanocomposite materials is not only influenced by the presence of the nanofiller in a rule-of-thumbs kind of way, but rather it is linked with other factors as well, making the final reinforcement quite complex to predict. One of these factors is crystal structure, which can greatly affect the mechanical properties of polymer-based materials. More specifically, it has been proposed that stiffness is significantly influenced by the crystallinity of the matrix [21-23, 47-50], while crystal size can be correlated with yield strength. [20-23]. The calculated crystallinity variations for all the prepared composites are presented in Fig. 3. A monotonously decreasing trend with increasing NDs content for every fixed MWCNTs concentration was revealed in every case. The same effect was observed in our previous work on PEX/NDs nanocomposites. Initially, for all the prepared composites with low NDs concentration, the crystallinity was found to be notably higher than PEX. As the nanofiller concentration increased, the crystallinity was found to be decreasing, reaching the same levels or in some cases marginally lower values compared to neat PEX. Thus, from this set of calculations it is confirmed that the amount of crystalline content of the composites can be directly correlated with their observed stiffness. It is noteworthy that the composite with the highest yield strength (PEX/2 wt% MWCNTs – 1 wt% NDs) had also the highest degree of crystallinity.

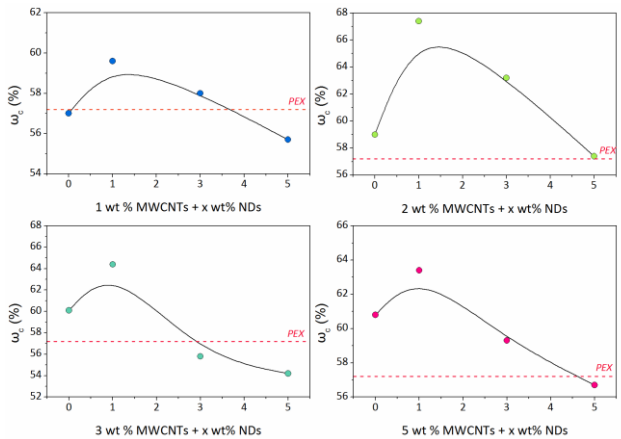

Fig. 3. Crystallinity values for all the prepared composites.

Regarding the influence of crystal size on the yield strength of the composites, the calculated values which are presented in Fig. 4, reveal that all the composites had larger crystal size, compared to the neat polymer. Even though a monotonously decreasing trend with increasing NDs concentration was not detected by these calculations, the fact that a larger mean crystal size was found for all of the composites, supports their enhanced yield strength [20-23]. Thus, the stiffness reinforcement, which is due to the presence of the fillers, seems to have a clear connection with the crystalline characteristics of the prepared nanocomposites. The higher crystallinity and enlarged crystals positively influence the stiffness of these composites.

It has been proposed that an increase in the yield strength can also be caused by a decrease of macromolecular chain mobility, and therefore, yield strength may serve as a qualitative measure of macromolecular chain mobility [51, 52]. In the present case we detected a higher yield strength and larger crystal size for all the nanocomposites, compared to the neat polymer, which can be rationalized in the following way: larger crystals lead to large

nanoconfined areas within the bulk of the polymer, in which macromolecular mobility is restricted [30-32], and hence, this can support the observed higher yield strength of the composites. Moreover, the larger crystals can bear more adequately the externally applied load, supporting a more efficient load transfer in the composites, due to the presence of the fillers [34].

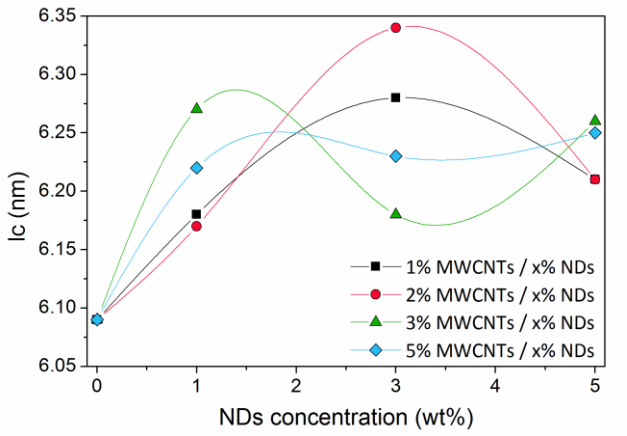

Fig. 4. Crystal size values for all the prepared composites.

Nanofiller-related factors affecting the mechanical properties of the composites

As filler-matrix adhesion and interactions are crucially influential factors in composites, the adhesion was evaluated through the application of Einstein's expression:

$$\frac{E_c}{E_m} = 1 + BV_f \quad (6)$$

where E_c and E_m are the elastic moduli of the composite and the polymer matrix respectively, V_f is the volume fraction of the fillers and B is a constant related to interfacial adhesion. When no adhesion exists between the matrix and the fillers, B becomes 1, while for strong adhesion, B becomes higher than 2.5 [53]. In general, the superior stiffness of MWCNTs and NDs can greatly affect the modulus and strength at yield of their composites when filler dispersion and filler-matrix adhesion are sufficient. The results, which are presented in Fig. 5 reveal that in order to successfully fit the experimental values, a decreasing adhesion parameter trend with increasing NDs concentration is required. In any case, the adhesion is significantly higher in the low NDs concentrations and declines as their content increases. This finding is in agreement with our previous work on PEX/NDs. Thus, in the case of mixed nanofillers as well, superior adhesion and better dispersion which lead to greatly enhanced stiffness are observed in the nanocomposites with minimum filler concentrations.

The intermolecular filler-matrix interactions can be indirectly evaluated through the liquid-solid surface interaction parameters, as calculated through the contact angle results analyses previously presented. In Table 2 the results of contact angle measurements and specific free energy analyses are summarized. For every set of composites, the contact angle values using water droplets were found to be higher than the corresponding one of neat PEX, in agreement with our previous findings on PEX/NDs composites [42]. Therefore, the weak hydrophilic nature of PEX was found to be converted to hydrophobic as a consequence of nanofillers incorporation, even if no straightforward increasing contact angle trend could be revealed.

For the PEX/1 wt% MWCNTs/1-5 wt% NDs composites, specific free energy as calculated using Fowkes' and Wu's formulas, was found to be increasing with increasing NDs content while remaining lower than neat PEX. The values of the dispersive and polar contributions to specific free energy calculated by using both methods are also listed in Table 2. The results reveal a clear trend caused by the NDs presence: while the dispersive forces clearly become higher when NDs concentration increases, the polar forces are almost eliminated. For all the other mixed-filler composites, similar conclusions can be drawn. The balance of dispersive and polar forces contribution to specific free energy follows the same scheme as in the previously discussed composites.

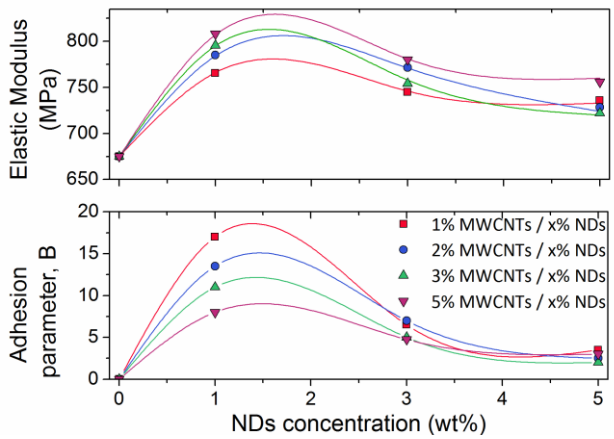

Fig. 5. Elastic modulus experimental (symbols) and fitted values (lines) using Einstein's model and adhesion parameter variation against NDs concentration.

In the case of the mixed nanocomposites, a straightforward correlation of the interfacial interactions with the measured strength and toughness is not always possible as was in the case with only NDs [42]. Due to the fact that the polar forces contribution to the specific free energy of the composites was found to be negligible, only the dispersive interactions parameter should be considered in such an investigation. A decreasing trend of the interaction parameter with increasing NDs content was detected in almost every set of composites. This finding may be explained by the fact that as filler content increases, more and larger filler aggregations are formed, as evidenced from the microscopy observations, leading to an overall lower matrix-filler interaction possibility.

The composite with 1 wt% MWCNTs/1 wt% NDs had the highest interaction parameter values, which implies that these enhanced interactions can support the superior ultimate strength and toughness found in this composite from the tensile experiments. Moreover, the general trend of decreasing dispersive interactions parameter with increasing NDs concentration which was found in all the composites, can also be correlated with their measured strength and toughness decrease. In some composites this behavior is less pronounced or not straightforward, like in the PEX/3 wt% MWCNTs/1-5 wt% NDs composites, but the general conclusion remains the same. Particularly for the PEX/3 wt% MWCNTs/1-5 wt% NDs composites, the fact that through TEM images presented in Fig.1d-f, the fillers aggregations were found to form large arrays, suggests that their mechanical behavior might be more complicated and affected mainly by filler dispersion. Similarly, the large filler aggregations which are formed in the PEX/5 wt% MWCNTs/1-5 wt% NDs composites suggest that their mechanical performance will most probably be governed by their poor dispersion and large aggregation state, rather than their seemingly high interaction parameter. Indeed, the dispersive interactions parameter variations

with NDs concentration cannot be linearly related to the measured significant decrease of the composites' toughness.

Table 2. Contact angles, specific free energy calculations using Fowkes' and Wu's methods and interaction parameter for all the prepared nanocomposites. (Negative contributions are considered as zero)

Material	Contact angle (°)		Fowkes Specific Free Energy contributions (J/m^2)			Wu Specific Free Energy contributions (J/m^2)			Interactions parameter
	Water	CH_2I_2	Total	Dispersive	Polar	Total	Dispersive	Polar	
Neat PEX	80.4±3.8	55.4±3.3	32.7±4.4	25.6±2.2	7.3±2.1	39.2±3.4	27.7±1.5	11.6±1.8	0.25
1 wt% MWCNTs – 1 wt% NDs	101.2±6.1	61.3±1.7	27.5±2.9	26.9±1.9	0.7±1.0	29.9±3.8	26.6±1.4	3.3±2.4	0.34
1 wt% MWCNTs – 3 wt% NDs	106.6±2.6	48.0±2.0	37.8±7.11	38.0±5.7	0.2±1.4	37.4±1.6	37.4±1.5	0.0±0.1	0.19
1 wt% MWCNTs – 5 wt% NDs	105.7±1.7	46.7±1.0	38±0.89	37.9±0.8	0.0±0.1	37.6±3.3	37.5±2.5	0.1±0.8	0.18
2 wt% MWCNTs – 1 wt% NDs	97.1±4.6	56.8±1.0	30±2.33	28.9±1.3	1.1±0.9	32.7±2.6	28.2±0.8	4.5±1.8	0.28
2 wt% MWCNTs – 3 wt% NDs	106.9±2	47.7±2.0	37.7±1.53	37.6±1.4	0.1±0.1	38.6±7.3	38.9±6.1	-0.4±1.3	0.19
2 wt% MWCNTs – 5 wt% NDs	102.5±1	47.7±0.9	36.4±0.68	36.4±0.6	0.0±0.6	36.0±1.1	34.4±0.7	1.6±0.4	0.19
3 wt% MWCNTs – 1 wt% NDs	87.5±4.5	58.5±1.5	29.8±3.37	25.4±1.5	4.4±1.9	35.2±2.7	26.6±0.8	8.7±1.9	0.29
3 wt% MWCNTs – 3 wt% NDs	110.2±2	46.4±1.7	39.8±1.55	39.4±1.3	0.4±0.3	35.0±1.6	30.0±0.8	5.0±0.8	0.19
3 wt% MWCNTs – 5 wt% NDs	104.5±1.3	51.5±1.4	34.2±1.06	34.2±1.1	0.0±0.1	34.1±1.7	33.0±1.1	1.1±0.5	0.23
5 wt% MWCNTs – 1 wt% NDs	103.6±1.2	56.1±1.2	31.2±0.96	31.0±0.9	0.1±0.1	31.9±1.3	30.0±0.8	1.9±0.5	0.28
5 wt% MWCNTs – 3 wt% NDs	109.4±3.6	51.3±2.0	36±1.92	35.8±1.7	0.1±0.3	35.0±2.4	30.0±1.0	5.0±1.4	0.23
5 wt% MWCNTs – 5 wt% NDs	111.5±1.3	57.2±1.2	32.4±0.98	32.3±0.9	0.1±0.1	28.7±18.5	29.8±16.3	-1.1±2.2	0.3

Fractography

In Fig. 6-9, characteristic fracture surfaces of the prepared nanocomposites are presented. The observations of the surfaces of these specimens reveal that for low filler concentrations some small and shallow micro-voids can be found in their rather smooth exterior. As the filler concentration increases, the surfaces become rougher and the voids larger and deeper. Moreover, for the lowest nanofiller concentrations the dense polymer fibrillar structure is retained. In these cases, the significant plastic deformation prior to failure was demonstrated by the highly elongated fibrils, which indicate that important amounts of energy were absorbed by the materials during deformation prior to failure. As nanofillers concentration increased, the fibrils were clearly more abruptly cut and had experienced lower deformation degrees suggesting a pre-mature failure before extensive deformation could take place. Also, the ductile to brittle transition as a consequence of the increasing filler concentration was evidenced by the fractography images. Shear banding was found to dominate the ductile fracture of some composites whereas crazing fracture features were found in all the more brittle composites. Furthermore, in some cases crack openings were found in the areas of large filler aggregates, suggesting that these act as stress concentrators and result in premature failure.

More specifically, the exterior of composites with low filler concentrations (Fig. 6a-b) appears rather smooth with the small and shallow crack openings. Higher filler concentrations (Fig. 6c-d) result in rougher surfaces dominated by notably larger and deeper cracks. A closer look-up of the outer surface of a PEX/1% MWCNTs-5%NDs specimen shown in Fig. 6d reveals a deep 600 μm crack opening along with other smaller cracks in the applied force direction. The large depth of the crack opening and the abrupt cut of the material's fibrils along with their small deformation degree can also be seen through that image.

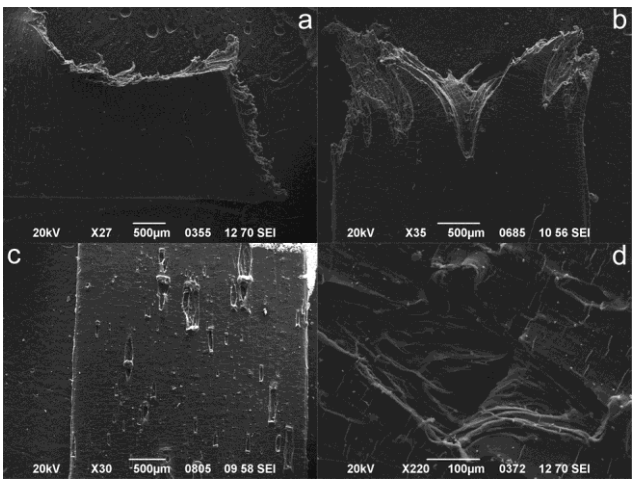

Fig. 6. Fractured specimens of PEX with: (a) 1% MWCNTs /1% NDs, (b) 2% MWCNTs /1% NDs, (c) 2% MWCNTs /5% NDs and (d) 1% MWCNTs /5% NDs.

Another critical factor which is changed as a consequence of filler concentration is the fibrillar density and the corresponding degree of fibrils' deformation prior to failure. As evidenced from Fig. 7a-b, the polymer's dense fibrillar structure was maintained for the low filler composites, while the fibrils appear to have experienced significant deformation prior to failure. This suggests that the main energy-absorbing mechanism, which is shear banding in these cases (Fig. 7a, 8a-b) is efficiently functioning thus allowing a large material strain response and a ductile performance [45]. As the filler concentration increased (Fig. 7c-h), the polymer fibrils appear to have been abruptly cut while experiencing a significantly smaller deformation degree. This observation points out that failure had

occurred fast, prior to notable deformation and therefore, these composites have a brittle fracture performance.

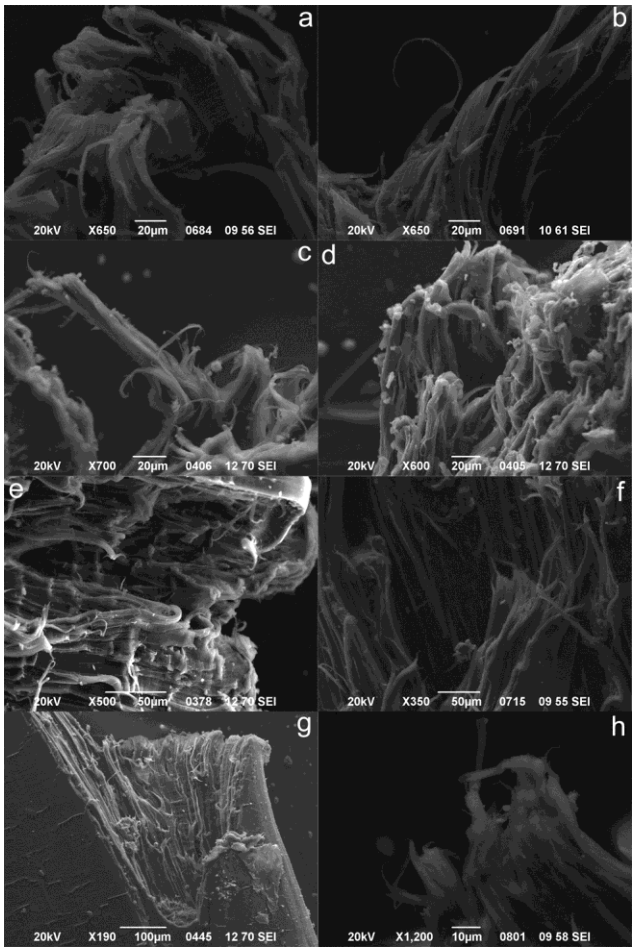

Fig. 7. Different fibrils' deformation degrees are shown in PEX composites with (a) 1% MWCNTs /1% NDs, (b) 2% MWCNTs /1% NDs, (c) 3% MWCNTs /5% NDs, (d) 3% MWCNTs /5% NDs, (e) 1% MWCNTs /5% NDs, (f) 5% MWCNTs /1% NDs, (g) 5% MWCNTs /5% NDs and (h) 1% MWCNTs /5% NDs.

Another major difference in the fracture behavior of the composites with low and higher filler loadings is their deformation mechanism. Apparently, for the low filler concentration composites, shear banding is the predominant deformation mechanism (Fig. 8a-b), while for higher filler loadings, crazing becomes the principle fracture mechanism (Fig. 8c-d). Shear banding can be related to the higher ductility of the samples with low filler content, while crazing denotes more brittle composites [45].

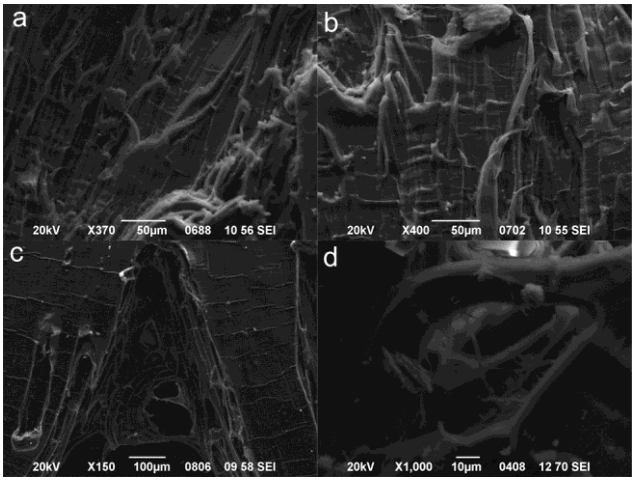

Fig. 8. Fracture micro-mechanism transition from (a-b) shear banding to (c-d) crazing in PEX nanocomposites with: (a) 2% MWCNTs /1% NDs, (b) 3% MWCNTs /1% NDs, (c) 2% MWCNTs /5% NDs and (d) 3% MWCNTs /5% NDs.

Through fractography observations, many nanotubes and polymer-covered nanotubes were found to either be hanging from the cut edges, or bridging the separated polymer lumps, thus highlighting the sufficient load transfer between the fillers and the matrix (Fig. 9a-c) as also suggested by other groups for polymer/nanotubes composites [54, 55].

In some composites with high filler content, the fractography observations indicate the possibility that fracture occurred in the nanoconfined filler-aggregation areas (Fig. 9d-f). The aggregates act as stress concentrators prohibiting the efficient load carrying over the formed cracks and thus, leading to lower toughness and premature failure. This is plausible as in the nanoconfined regions the fluctuating density and hindered chain mobility can lead to severely different deformations of the molecular chains and therefore, premature failure [44]. The images also reveal that in the highly loaded composites, the surrounding matrix in the crack opening is not severely deformed (Fig. 7e, 7g, 8d, 9d), confirming that crack coalescence progressed rather fast, before significant strain was achieved.

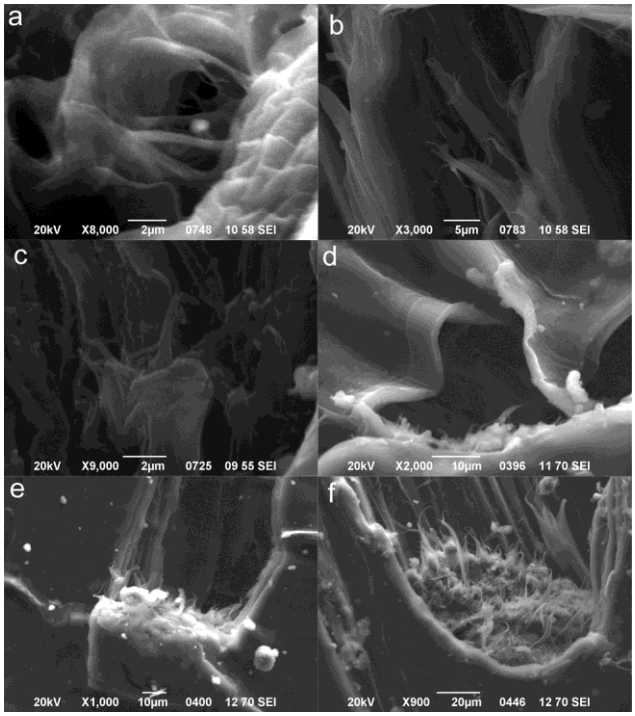

Fig. 9. Failure at aggregates-rich areas in PEX nanocomposites with: (a) 1% MWCNTs /2% NDs, (b) 5% MWCNTs /3% NDs, (c) 5% MWCNTs /1% NDs, (d) 3% MWCNTs /5% NDs, (e) 3% MWCNTs /5% NDs and (f) 5% MWCNTs /5% NDs.

Therefore, from the study of the stretched specimens of the mixed composites, it was confirmed that increasing filler content leads to a toughness decrease and a more pronounced embrittlement of the polymer. It was also suggested that the premature failure occurs in the large filler aggregations which constitute stress concentrators. The tensile testing finding that increasing filler concentration leads to a ductile to brittle transition in the composites was confirmed and related to a micro-deformation mechanism transformation, from shear banding to crazing.

Thermal properties

In Table 3, the thermal properties of the composites, their thermal diffusivity (α), specific heat capacity (C_p) and thermal conductivity (κ) are presented. A clear thermal conductivity enhancement was revealed for all the studied nanocomposites which was found to be enhanced with increasing NDs concentration for every set of composites with fixed MWCNTs content. The smallest detected thermal conductivity enhancement compared to the neat polymer was 100%. The highest thermal conductivity values were observed in the group of PEX/3 wt% MWCNTs/x wt% NDs, suggesting that the conductivity of the nanocomposites is not linearly related to their nanofiller concentration. While a modest increase was found in the thermal diffusivity values of all the composites, their significantly enhanced specific heat capacity values denote that the observed thermal conductivity boost can be related with the ability of the composites to absorb higher amounts of heat for the same temperature difference. From a systematic thermal conductivity study of PEX/MWCNTs and PEX/NDs composites reported in our previous work [42, 56], it was found that these fillers contribute differently to the observed thermal conductivity increase. While MWCNTs significantly enhance the C_p of the composites and also cause a modest increase on their thermal diffusivity, NDs only enhance the C_p resulting in a slightly more significant final conductivity increase. In the mixed composites however, the results clearly indicate that a standard cumulative behavior of the independent effects of each type of filler cannot be proposed. The observed aggregations formed by both of these fillers shown in Fig. 1, support the thermal conductivity finding that the effects of the presence of both MWCNTs and NDs cannot be a linear cumulative drift of the effects of each type of filler. Thus, a collective response of mixed MWCNTs and NDs regarding the thermal transport properties of the prepared composites seems to explain the observed thermal conductivity boost.

Such a reinforcement combined with improved mechanical performance can be considered substantially satisfactory from an industrial point of view since, e.g. in an under-floor piping installation a thermal conductivity increase higher than 50% leads to an overall cost depreciation in less than two years.

Table 3. Thermal Properties of the prepared materials

Material	Thermal Diffusivity (mm^2/s)	C_p (J/g K)	Thermal Conductivity (W/m K)
Neat PEX	0.165 ± 0.001	1.18 ± 0.09	0.17 ± 0.010
1 wt% MWCNTs – 1 wt% NDs	0.175 ± 0.002	2.23 ± 0.04	0.34 ± 0.005
1 wt% MWCNTs – 3 wt% NDs	0.179 ± 0.001	2.47 ± 0.02	0.41 ± 0.005
1 wt% MWCNTs – 5 wt% NDs	0.191 ± 0.002	2.43 ± 0.04	0.44 ± 0.080
2 wt% MWCNTs – 1 wt% NDs	0.183 ± 0.001	2.21 ± 0.17	0.38 ± 0.030
2 wt% MWCNTs – 3 wt% NDs	0.192 ± 0.002	2.20 ± 0.04	0.38 ± 0.005
2 wt% MWCNTs – 5 wt% NDs	0.185 ± 0.001	2.50 ± 0.18	0.42 ± 0.035
3 wt% MWCNTs – 1 wt% NDs	0.177 ± 0.002	2.62 ± 0.06	0.43 ± 0.010
3 wt% MWCNTs – 3 wt% NDs	0.178 ± 0.001	2.76 ± 0.07	0.44 ± 0.010
3 wt% MWCNTs – 5 wt% NDs	0.182 ± 0.001	2.58 ± 0.21	0.45 ± 0.035
5 wt% MWCNTs – 1 wt% NDs	0.191 ± 0.001	2.00 ± 0.31	0.34 ± 0.050
5 wt% MWCNTs – 3 wt% NDs	0.187 ± 0.002	2.18 ± 0.21	0.38 ± 0.040
5 wt% MWCNTs – 5 wt% NDs	0.183 ± 0.001	2.34 ± 0.42	0.38 ± 0.070

In Fig. 10a the mass loss curves of the nanocomposites with 1 wt% MWCNTs/1-5 wt% NDs are presented. An obvious progressive increase in the thermal stability was found with increasing NDs content, presenting the same trend as the one detected regarding the thermal conductivity of the composites. The temperatures at which the sample has experienced a mass loss of 0.5 and 1% respectively, denoted as $T_{0.5}$ and T_1, are often used as thermal stability indications. In the present case, a progressive increase of 16.9, 26.7 and 28.7 ^oC was found for the $T_{0.5}$ with increasing NDs concentration, while the corresponding increase of T_1 was 12.7, 21 and 26 ^oC respectively. The observed progressive significant thermal stability enhancement can be attributed to the formation of more nanoconfined regions around the nanofillers, in which the local density fluctuations and hindered macromolecular chain mobility lead to a chemical reactivity decrease [30]. Therefore, it is reasonable that an increased filler concentration would lead to a thermal stability increase. The mass residue of the measured samples also follows the expected increasing trend as the nanofillers are left as solid residues while polymer decomposes completely.

In Fig. 10b the mass loss curves of the nanocomposites with 2 wt% MWCNTs/1-5 wt% NDs are presented. Again, a noteworthy enhancement of the thermal stability can be seen in all of these composites. Even though the differences in the mass loss curves of PEX/2 wt% MWCNTs/3wt% NDs and PEX/2 wt% MWCNTs/5 wt% NDs are extremely small, a clear thermal stability increase can be seen both of them. In details, the $T_{0.5}$ increase was found to range between 10.8-19.6 ^oC for the three composites while the T_1 increase was 11-14.3 ^oC . The mass residue also confirmed the presence of the nanofillers in the matrix.

In Fig. 10c the mass loss curves of the nanocomposites with 3 wt% MWCNTs/1-5 wt% NDs are shown, presenting the highest thermal stability enhancement found in the studied composites. Even though the differences between the mass loss curves of the three composites are very small, they still point out the significant effect that the combination of MWCNTs and NDs have on PEX matrix. The measured $T_{0.5}$ increase was 20.5, 33.1 and 35.2 ^oC for increasing NDs concentration while T_1 increased 16.3, 24.6 and 26.5 ^oC respectively. In this case also the mass residue was found to follow the expected increasing trend with increasing filler content. It is noteworthy that these particular composites presented the more significantly enhanced thermal stability and thermal conductivity of all the composites.

Finally, the mass loss curves of PEX/5 wt% MWCNTs/1-5 wt% NDs composites are shown in Fig. 10d revealing again a notable thermal stability enhancement of PEX. The $T_{0.5}$ increase varied between 9.5-16.5 ^oC while the T_1 increase ranged between 6.3-13.7 ^oC. In this case also the final residues of the measured samples followed the expected increasing trend with increasing filler content. Therefore, from the thermogravimetry measurements, it was revealed that the presence of MWCNTs and NDs leads to a great enhancement of the thermal stability of PEX, which can be explained in the framework of the increased nanoconfined areas within the matrix.

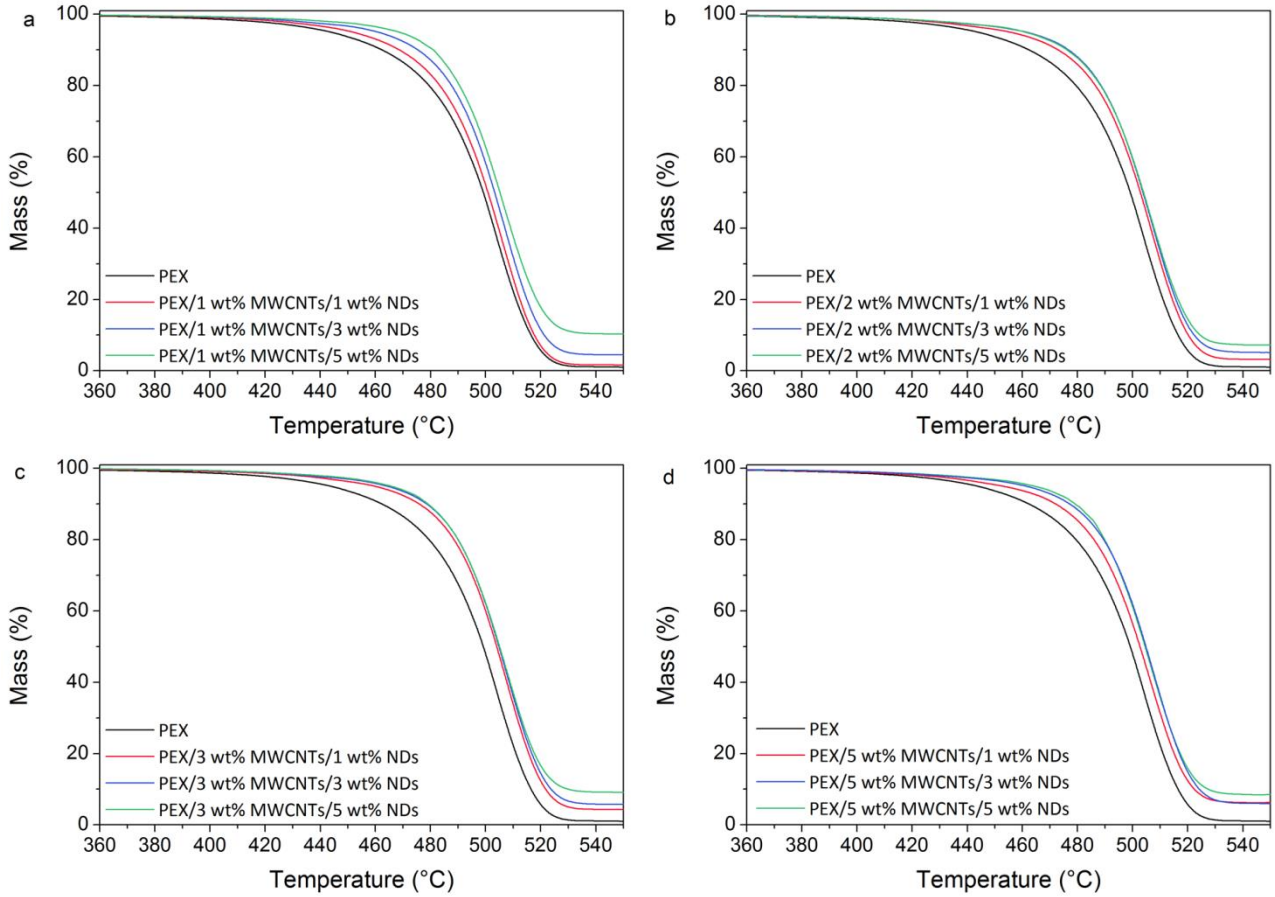

Fig. 10. Mass loss curves of PEX composites with (a) 1 wt% MWCNTs/1-5 wt% NDs, (b) 2 wt% MWCNTs/1-5 wt% NDs, (c) 3 wt% MWCNTs/1-5 wt% NDs, (d) 5 wt% MWCNTs/1-5 wt% NDs, heated at 20K min^{-1} in N_2 flow.

Conclusions

Crosslinked polyethylene nanocomposites with small amounts of MWCNTs and NDs were prepared by solid state ball milling and subsequent melt-mixing. Their mechanical and thermal properties reinforcement was thoroughly examined. The systematic investigation of the morphology, structure and mechanical performance of the prepared mixed nanocomposites revealed a notable stiffness enhancement, while ultimate strength and toughness were found to only slightly increase in minimum filler concentrations. This was attributed to the fact that only in minimum filler content a satisfactory dispersion and adhesion can be achieved, thus allowing the successful reinforcement of the matrix in every aspect. As the nanofiller content increased, the formed aggregates enlarged and the interactions with the matrix were poorer, leading to a more brittle performance. A direct connection between crystalline features (crystallinity and crystal size), macromolecular conformation and macroscopic properties has been proposed. The crystalline characteristics of the composites mainly affected their stiffness, which was decreasing with increasing NDs content. Even though the mixed composites had a notably higher stiffness compared to neat PEX, their overall reinforcement was less significant compared to the composites with only one type of filler. From the observation fracture surfaces of the composites, a toughness and ultimate strength decrease with increasing filler content was confirmed and supported by the decreasing adhesion and poorer filler dispersion in the higher filler loadings.

From the thermal behavior of the mixed composites, a modest increase in thermal diffusivity and a notable increase in specific heat capacity with increasing NDs concentration were found to yield a significant thermal conductivity improvement. Furthermore, the presence of MWCNTs and NDs led to a great enhancement of the thermal stability of PEX, which can be explained in the framework of the increased nanoconfined areas within the matrix.

Acknowledgements

The authors wish to acknowledge co-funding of this research by European Union- European Regional Development Fund and Greek Ministry of Education/EYDE-ETAK through program ESPA 2007-2013 / EPAN II / Action "SYNERGASIA" (project 09SYN-33-484).
The authors would also like to thank Prof. Aldo Boccaccini of the University of Erlangen-Nurnberg for allowing the use of the contact angle facilities available at Biomaterials Department.

Notes and references

[a] Solid State Physics Section, Physics Department, Aristotle University of Thessaloniki, 541 24 Thessaloniki, Greece.
[b] Polymers' Laboratory, Department of Materials Science Engineering, University of Ioannina, University Campus, 45110 Ioannina, Greece.
[c] Department of Mechanical and Manufacturing Engineering, University of Cyprus, 1678 Nicosia, Cyprus .

[d] Laboratory of Polymer Chemistry and Technology, Department of Chemistry, Aristotle University of Thessaloniki, 541 24 Thessaloniki, Greece.

1. S. Pavlidou and C. D. Papaspyrides, *Progress in Polymer Science*, 2008, 33, 1119-1198.
2. N. G. Sahoo, S. Rana, J. W. Cho, L. Li and S. H. Chan, *Progress in Polymer Science*, 2010, 35, 837-867.
3. M. R. Loos and K. Schulte, *Macromolecular Theory and Simulations*, 2011, 20, 350-362.
4. J. N. Coleman, U. Khan and Y. K. Gun'ko, *Advanced Materials*, 2006, 18, 689-706.
5. S. C. Tjong, *Energy & Environmental Science*, 2011, 4, 605-626.
6. B. Chen, J. R. G. Evans, H. C. Greenwell, P. Boulet, P. V. Coveney, A. A. Bowden and A. Whiting, *Chemical Society Reviews*, 2008, 37, 568-594.
7. G. Keledi, J. Hari and B. Pukanszky, *Nanoscale*, 2012, 4, 1919-1938.
8. Y. Kojima, A. Usuki, M. Kawasumi, A. Okada, Y. Fukushima, T. Kurauchi and O. Kamigaito, *Journal of Materials Research*, 1993, 8, 1185-1189.
9. C. Jiang, A. Saha, C. C. Young, D. P. Hashim, C. E. Ramirez, P. M. Ajayan, M. Pasquali and A. A. Martí, *ACS Nano*, 2014, DOI: 10.1021/nn502552q.
10. C. Xiang, W. Lu, Y. Zhu, Z. Sun, Z. Yan, C.-C. Hwang and J. M. Tour, *ACS Applied Materials & Interfaces*, 2011, 4, 131-136.
11. N. Behabtu, C. C. Young, D. E. Tsentalovich, O. Kleinerman, X. Wang, A. W. K. Ma, E. A. Bengio, R. F. ter Waarbeek, J. J. de Jong, R. E. Hoogerwerf, S. B. Fairchild, J. B. Ferguson, B. Maruyama, J. Kono, Y. Talmon, Y. Cohen, M. J. Otto and M. Pasquali, *Science*, 2013, 339, 182-186.
12. C. Gao, S. Zhang, B. Han, H. Sun, G. Wang and Z. Jiang, *RSC Advances*, 2014, DOI: 10.1039/C4RA07473D.
13. R. Krishnamoorti, R. A. Vaia and E. P. Giannelis, *Chemistry of Materials*, 1996, 8, 1728-1734.
14. E. P. Giannelis, *Applied Organometallic Chemistry*, 1998, 12, 675-680.
15. C. Liu, J. Ma, X. Gan, R. Li and J. Wang, *Composites Science and Technology*, 2012, 72, 915-923.
16. B. Zhang, M.-H. Lee, A. N. Chakoli, W. Zang, K. Zhang, Y. Zhang, G. Song, C. Chen, X. Li and Y. Li, *RSC Advances*, 2014, 4, 14024-14030.
17. L. Chen, D. Rende, L. S. Schadler and R. Ozisik, *Journal of Materials Chemistry A*, 2013, 1, 3837-3850.
18. M. H. Wang, W. H. Ruan, Y. F. Huang, L. Ye, M. Z. Rong and M. Q. Zhang, *Journal of Materials Chemistry*, 2012, 22, 4592-4598.
19. P. Xu, X. Han, B. Zhang, Y. Du and H.-L. Wang, *Chemical Society Reviews*, 2014, 43, 1349-1360.
20. X. C. Zhang, M. F. Butler and R. E. Cameron, *Polymer*, 2000, 41, 3797-3807.
21. O. Darras and R. Séguéla, *Journal of Polymer Science Part B: Polymer Physics*, 1993, 31, 759-766.
22. B. A. G. Schrauwen, R. P. M. Janssen, L. E. Govaert and H. E. H. Meijer, *Macromolecules*, 2004, 37, 6069-6078.
23. J. M. Schultz, *Polymer Engineering & Science*, 1984, 24, 770-785.
24. S. A. Meguid and Y. Sun, *Materials & Design*, 2004, 25, 289-296.
25. M. Fowkes Frederick, in *Contact Angle, Wettability, and Adhesion*, AMERICAN CHEMICAL SOCIETY, 1964, vol. 43, ch. 6, pp. 99-111.
26. I. U. S. Lipatov, *Polymer Reinforcement*, ChemTec, 1995.
27. J. Roesler, H. Harders and M. Baeker, *Mechanical Behaviour of Engineering Materials: Metals, Ceramics, Polymers, and Composites*, Springer, 2007.
28. M. M. Elmahdy, K. Chrissopoulou, A. Afratis, G. Floudas and S. H. Anastasiadis, *Macromolecules*, 2006, 39, 5170-5173.
29. S. H. Anastasiadis, K. Chrissopoulou and B. Frick, *Materials Science and Engineering: B*, 2008, 152, 33-39.
30. K. Chen, C. A. Wilkie and S. Vyazovkin, *The Journal of Physical Chemistry B*, 2007, 111, 12685-12692.
31. F. W. Starr, T. B. Schrøder and S. C. Glotzer, *Macromolecules*, 2002, 35, 4481-4492.
32. V. A. Harmandaris, K. C. Daoulas and V. G. Mavrantzas, *Macromolecules*, 2005, 38, 5796-5809.
33. E. Roumeli, K. M. Paraskevopoulos, D. Bikiaris and K. Chrissafis, *J Mater Sci*, 2013, 48, 6753-6761.
34. R. O. Ebewele, *Polymer Science and Technology*, Taylor & Francis, 2000.
35. G. Akovali and A. Atalay, *Polym Test*, 1997, 16, 165-171.
36. B. Wunderlich, *Macromolecular Physics: Crystal nucleation, growth, annealing*, Academic Press, 1976.
37. B. Wunderlich and G. Czornyj, *Macromolecules*, 1977, 10, 906-913.
38. J. D. Hoffman, *Polymer*, 1982, 23, 656-670.
39. S. Wu, *J Polym Sci Part C: Polym Symp*, 1971, 34.
40. L. A. Girifalco and R. J. Good, *The Journal of Physical Chemistry*, 1957, 61, 904-909.
41. E. Roumeli, E. Pavlidou, D. Bikiaris and K. Chrissafis, *Carbon*, 2014, 67, 475-487.
42. E. Roumeli, E. Pavlidou, A. Avgeropoulos, G. Vourlias, D. N. Bikiaris and K. Chrissafis, *Submitted manuscript in the Journal of Physical Chemistry Part B, ACS Publications*.
43. M. Tanniru, Q. Yuan and R. D. K. Misra, *Polymer*, 2006, 47, 2133-2146.
44. E. P. Giannelis, R. Krishnamoorti and E. Manias, in *Polymers in Confined Environments*, eds. S. Granick, K. Binder, P. G. Gennes, E. P. Giannelis, G. S. Grest, H. Hervet, R. Krishnamoorti, L. Léger, E. Manias, E. Raphaël and S. Q. Wang, Springer Berlin Heidelberg, 1999, vol. 138, ch. 3, pp. 107-147.
45. H. F. Mark, *Encyclopedia of Polymer Science and Technology, Concise*, Wiley, 2013.
46. Q. Yuan and R. D. K. Misra, *Polymer*, 2006, 47, 4421-4433.
47. A. Pawlak, A. Galeski and A. Rozanski, *Progress in Polymer Science*, DOI: http://dx.doi.org/10.1016/j.progpolymsci.2013.10.007.
48. T. Kazmierczak, A. Galeski and A. S. Argon, *Polymer*, 2005, 46, 8926-8936.
49. N. W. J. Brooks and M. Mukhtar, *Polymer*, 2000, 41, 1475-1480.
50. P. A. O'Connell and G. B. McKenna, in *Encyclopedia of Polymer Science and Technology*, John Wiley & Sons, Inc., 2002, DOI: 10.1002/0471440264.pst463.
51. A. Galeski, Z. Bartczak, T. Kazmierczak and M. Slouf, *Polymer*, 2010, 51, 5780-5787.
52. J. D. Ferry, *Viscoelastic Properties of Polymers*, Wiley, 1980.
53. L. Zhou, C. Gao and W. Xu, *Journal of Materials Chemistry*, 2010, 20, 5675-5681.
54. P. M. Ajayan, L. S. Schadler, C. Giannaris and A. Rubio, *Advanced Materials*, 2000, 12, 750-753.
55. Z. Bartczak, A. Galeski, A. S. Argon and R. E. Cohen, *Polymer*, 1996, 37, 2113-2123.
56. E. Roumeli, A. Markoulis, T. Kyratsi, D. Bikiaris and K. Chrissafis, *Polymer Degradation and Stability*, 2014, 100, 42-53.